electronics

MDPI

Article

Folded Narrow-Band and Wide-Band Monopole Antennas with In-Plane and Vertical Grounds for Wireless Sensor Nodes in Smart Home IoT Applications

Mohammad Mahdi Honari [1,†], Seyed Parsa Javadi [2,†] and Rashid Mirzavand [2,*]

[1] Electrical & Computer Engineering, University of Wisconsin-Madison, Madison, WI 53706, USA
[2] Intelligent Wireless Technologies, University of Alberta, Edmonton, AB T6G 1H9, Canada
* Correspondence: mirzavan@ualberta.ca
† These authors contributed equally to this work.

Abstract: This article presents two monopole antennas with an endfire radiation pattern in the UHF band that can be installed on dry walls or metallic cabinets as a part of wireless sensor nodes, making them a suitable choice for smart home applications, such as the wireless remote control of house appliances. Two different antennas are proposed to cover the RFID bands of North America (902–928 MHz) and worldwide (860–960 MHz). The antennas have wide horizontal radiation patterns that provide great reading coverage in their communication with a base station placed at a certain distance from the antennas. The structures have two ground planes, one in-plane and the other vertical. The vertical ground helps the antenna to have a directive radiation and also makes it easily installed on walls. The antenna feeding line lies over the vertical ground substrate. The maximum dimensions of the narrow-band antenna are L × W = 0.3λ × 0.14λ, and those for the wide-band antenna are L × W = 0.39λ × 0.14λ. The measured results show that the bandwidth of the proposed antennas for the North America and worldwide RFID bands are from 902 MHz to 939 MHz and 822 MHz to 961 MHz, with maximum gains of 4.2 dBi and 4.9 dBi, respectively.

Keywords: monopole antenna; wide-band antenna; smart home; endfire radiation

check for updates

Citation: Honari, M.M.; Javadi, S.P.; Mirzavand, R. Folded Narrow-Band and Wide-Band Monopole Antennas with In-Plane and Vertical Grounds for Wireless Sensor Nodes in Smart Home IoT Applications. *Electronics* **2024**, *13*, 2262. https://doi.org/10.3390/electronics13122262

Academic Editors: Djuradj Budimir, Shaoqiu Xiao, Kai-Da Xu, Xiongying Liu and Yi Fan

Received: 20 April 2024
Revised: 28 May 2024
Accepted: 5 June 2024
Published: 8 June 2024

Copyright: © 2024 by the authors. Licensee MDPI, Basel, Switzerland. This article is an open access article distributed under the terms and conditions of the Creative Commons Attribution (CC BY) license (https://creativecommons.org/licenses/by/4.0/).

1. Introduction

With the advancement of the Internet of Things (IoT), smart sensing systems have become essential for home and industrial applications [1]. These systems are used for improving safety, monitoring the environment, and controlling the status of all parameters [2–4]. Key features necessary in the development of wireless sensors are low fabrication cost and small footprint. An antenna, as one of the largest components in sensing architectures, needs to be appropriately designed to perform well and to be cost-effective. Basically, sensor tags can be either active or passive. In the active sensors design, the sensor needs a battery to be functional, which leads to higher design complexity [5]. However, with the help of the battery power, the sensor can provide a longer reading range with a small antenna. Therefore, the antenna profile is not a challenging issue in the design of active sensors, while in battery-less wireless sensor nodes, or passive ones, the antenna is required to be low-profile with a suitable radiation gain [6].

Sensing tags are used in a wide range of applications, such as healthcare, environment monitoring, supply chain management and items identification in shopping centers [7], electronic transportation payment cards, smart homes, etc. In order to gain a general understanding of how an RFID tag operates, it is useful to mention two practical examples. Respiration measurement is a good example of a healthcare sensor. It utilizes the Doppler effect measured by a sensor tag. For this purpose, an RFID tag can be attached to the patient's chest, and an RFID reader be placed in the vicinity of the patient. The reader sends an EM signal to the tag, and the tag responds back. While breathing, the tag moves

with the chest movements, so the reflected signal undergoes a frequency shift due to the Doppler effect. The reader detects this frequency shift and then it can process the respiration rate [8]. For the environment monitoring application, one method is to put a small antenna tag inside a lake water sample as a probe and detect the ions dissolved in the water by measuring the change in the antenna reflection coefficient, S11 [9].

In North America, a variety of frequency bands are used for different RFID applications. They include the LF band, which provides access within 125–134 KHz, the HF band within 13.56 MHz, and the UHF band within 902–928 MHz. Each band serves a variety of applications. For example, the LF band is used for cases with low scanning ranges and data rates, because for short ranges, a small antenna is able to transmit or receive simple signals. Some examples for LF applications are access control and identification systems for buildings, cars, and shopping stocks, most of which obviously can be controlled and managed with low data rates and reading ranges [10].

When longer reading ranges and higher data rates are required, designers can move toward HF and UHF bands. There are several reasons why HF and UHF bands are preferred to LF bands in smart home applications. For example, with a higher frequency of operation, the designer can separate and manage the channels of smart household items with minimum interference. As well as this minimum interference, the user can have wider control over household items with higher data rates [10].

Based on the cases considered inside a smart home, one can choose between HF and UHF bands. In some applications, HF is advantageous over UHF. For example, in cases when the data security matters, an HF device can provide data connection within a close proximity, due to its short range in comparison with a UHF device [11]. Also, a house is essentially divided into different rooms by separating walls; therefore, a device sometimes needs to be controlled from the other rooms. Here, an HF design can be helpful, especially in metal housings, since HF waves are better able to penetrate walls than UHF waves [12].

However, the use of a UHF band is inevitable in a smart home design because of its high data rate and small antenna size and, last but not least, data should not leak outside from the house walls, which are providing a private environment for the house members [10]. Here, we are going to introduce two UHF monopole antennas used for smart home sensor applications, based on North American standards.

Since the sensing tags for smart home applications are usually installed on walls or cabinets, the antenna radiation pattern is required to be in the horizontal direction. In addition to compactness and excellent radiation performance, the tag antenna should have great coverage in the horizontal direction in order to have an extensive reading range in its communication with a randomly located base station (reader). In our recently published work [13], a battery-less RFID flood sensor was designed in the UHF band for smart home automation. In that work, a conventional patch antenna was used as the radiator that made the whole structure quite bulky. However, for practical applications, compact antennas with a wide horizontal radiation pattern are required to be used in wireless sensor nodes. Here, the proposed antenna utilizes a monopole configuration, offering more compactness when compared with a patch design. This antenna could be easily packaged together in a compact form with the transceiver circuit and is usually placed inside a home in an array of sensors, connected to a central hub, as shown in Figure 1. In this figure, each sensor measures a physical feature and sends its data to the central hub. Then, based on the received data, the hub commands other sensors to make a change in the house environment. In other words, the sensors close control feedback loops, the combination of which forms the whole smart home network.

The variety of RFID tag antennas and filters is quite diverse, and promising ideas can be found among different antenna types [14,15]. Specifically, various configurations of monopole antennas are introduced for RFID tag applications in the literature [16–18], but many of them do not provide enough bandwidth or directivity and also are not easy to assemble for smart home applications. Basically, it is not easy to attach endfire antennas to walls in sensor or imaging applications. In the antennas proposed in this document, the

vertical ground plane can provide a number of features. First, it provides a directive endfire radiation for the antenna; second, it makes the circuit easily attachable on a smart house wall; and third, the backside of the vertical ground substrate can be used as a place for the remaining RFID circuit to be assembled on, so the transceiver circuit can be simply isolated from the antenna leakage. The antenna feeding line is lying over the vertical ground substrate, connected to an external SMA connector. Last but not least, these antennas are suitable for passive battery-less design, according to the points mentioned before. Several other designs have also been created for the same purpose in the literature [19–21]. For example, Weng et al. [19] have designed a well-operating but complex RFID antenna for the North American band.



Figure 1. An array of sensors connected to a central hub, forming a smart home network.

In this article, the design of compact antennas has been addressed with an endfire radiation pattern in the UHF band to be used in battery-less RFID sensor nodes. Two different antennas are designed for the RFID bands of North America (902–928 MHz) and worldwide (860–960 MHz). Two resonances are created in the design of the worldwide RFID antenna to make it wide-band. The experimental tests were carried out, and the results show that maximum measured endfire radiation gains of 4.2 and 4.9 dBi are achieved for narrow-band and wide-band antennas, respectively.

2. Antenna Design

Because of their large size, microstrip patch antennas are not a good candidate to be used in RFID sensor nodes. Although a conventional dipole antenna has great coverage, it is also not a suitable choice for RFID sensor tags because of its backward radiation, relatively lengthy structure, and low antenna gain. However, monopole antennas are a type of antenna with a unidirectional endfire pattern and small size. In comparison with dipole antennas, monopole antennas can provide higher antenna gain and larger front-to-back (F/B) ratio, since they use a conductor as the ground at the back of the radiator [22]. In these antennas, to miniaturize the antenna size, folded or meandered structures can be used [23–26].

Figure 2 represents two folded monopole antennas with the in-plane ground and vertical ground. The antennas consist of a folded trace and an L-shaped ground plane. In the antenna with an in-plane ground surface, the sensing structure and the antenna trace are on the same plane. Basically, the sensing circuit is a transceiver circuit including filters, active parts, and maybe energy-harvesting sections, used for power saving. However, in the antenna with a vertical ground plane, the antenna trace and the sensing circuits are on

two orthogonal planes. The antenna in the latter case is more suitable for a wireless sensor node since the presence of an object on which the sensor will be mounted does not degrade the antenna performance. Moreover, in the case of the antenna with a vertical ground plane, the radiation of the antenna does not affect the sensing circuits, since the circuit structure is at the back of the antenna ground plane. This is very important for sensitive circuits such as the battery-less sensors reported in [13], which work based on the phase modulation of reflected signals. One great feature of the proposed antennas in Figure 2 is that the 3 dB beam width of the antennas in the horizontal direction is very large, which results in great coverage in their communication with the RFID reader.

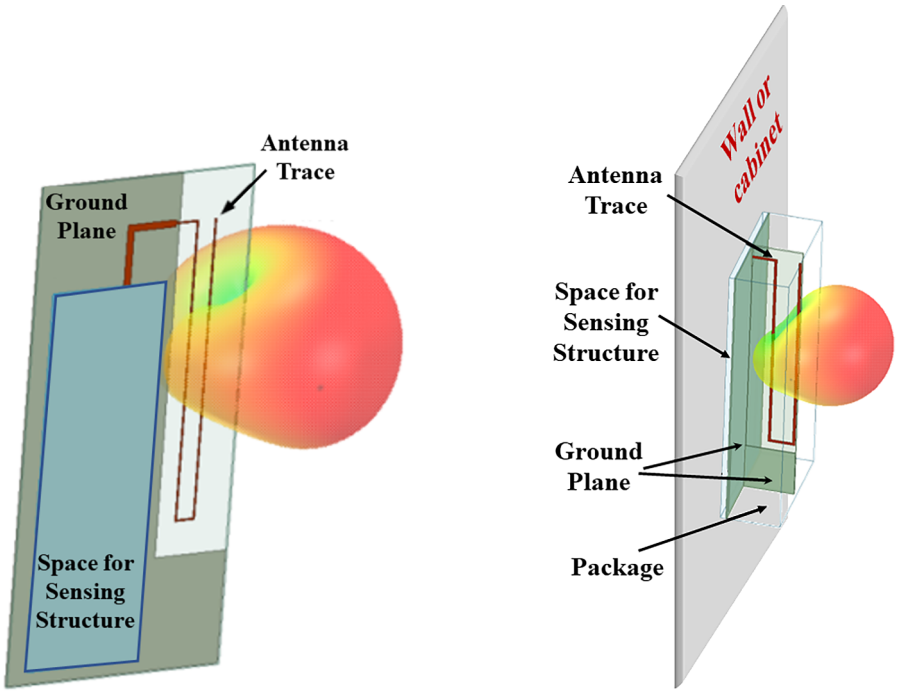


Figure 2. Monopole antennas with sensing circuits: (**a**) antenna with in-plane ground, and (**b**) antenna with vertical ground.

Figure 3 shows different views of two proposed narrow-band and wide-band monopole antennas. They are fabricated on pieces of FR-4 substrates with a permittivity, loss tangent, and thickness of 4.6, 0.02, and 0.7 mm, respectively. For the antenna of Figure 3a, the length of the trace (Lt) mainly determines the resonant frequency; therefore, the antenna is narrow-band. This antenna is designed to cover the RFID band of North America (902–928 MHz). The design parameters of the narrow-band antenna are L = 100 mm, W = 48 mm, Lt = 77 mm, Wt = 5 mm, Ls = 18.5 mm, Ts = 32 mm, g = 2 mm, d = 16 mm, and s = 6 mm. On the other side, the antenna in Figure 3b can provide a wide-band performance for by having two separate paths for the surface current flow. This antenna is designed to cover the worldwide RFID band (860–960 MHz). Adding a second branch to the antenna helps to create a wide-band design. The lengths of these two poles are optimized to bring two resonance frequencies close together, leading to a wide-band radiation. One branch of this antenna is shortened to the ground to increase its overall bandwidth. For the wide-band antenna, the designed parameters are L = 130 mm, W = 48 mm, Lf = 86 mm, Lt1 = 122 mm, Lt2 = 82 mm, Ls = 1 mm, Wt = Wf = 5 mm, Xf = 6 mm, g = 4.5 mm, d = 16 mm, and s = 6 mm.

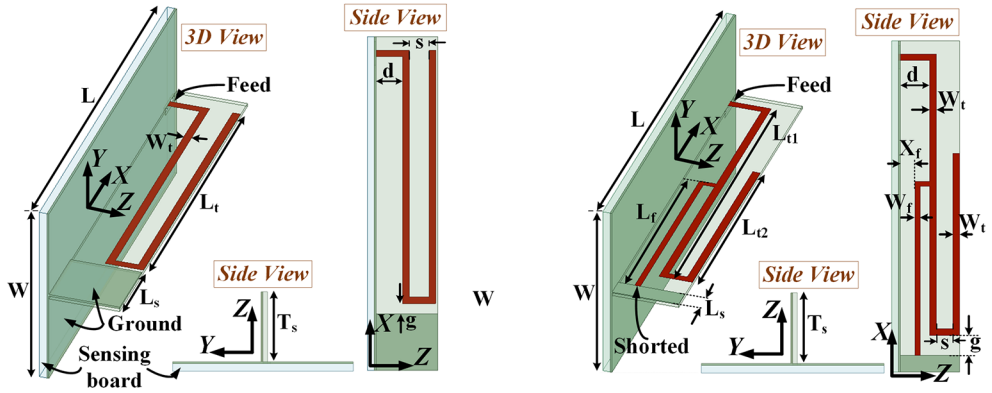


Figure 3. Proposed antenna structures, (**a**) narrowband antenna, and (**b**) wideband antenna.

To investigate the effect of main parameters on the proposed antennas' performance, parametric studies are performed in Figures 4 and 5. It is evident that the length of the antenna trace mainly adjusts the resonant frequency in the design of the narrow-band antenna in Figure 4a. However, the length of the ground plane also affects the resonant frequency, as investigated in Figure 4. As shown in Figure 4a, increasing the length of the antenna trace, i.e. Ls, downshifts the resonant frequency. It can also improve the reflection coefficient at the cost of smaller bandwidth. The ground plane behind the antenna trace, however, can improve the reflection coefficient without significant changes in the resonant frequency, as indicated in Figure 4b. As shown, for L = 100 mm, the antenna bandwidth covers the desired RFID band of North America. By increasing L, we may obtain a broader bandwidth at the cost of larger antenna size. To study the wide-band operation of the proposed antenna in Figure 3b, the two main parameters affecting the reflection coefficient of the wide-band antenna are investigated in Figure 5.

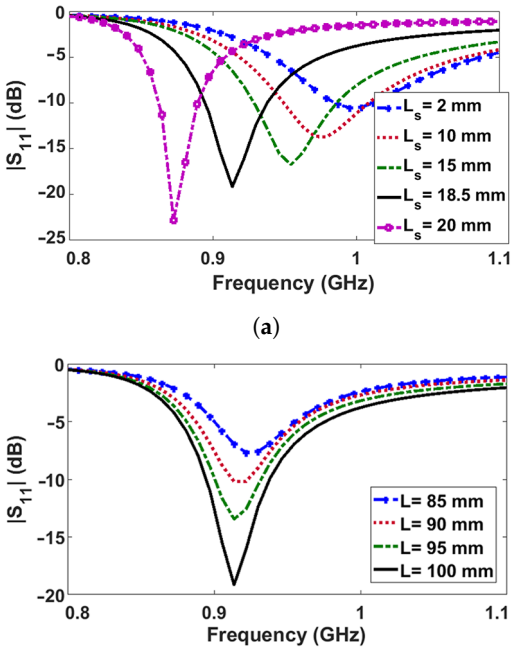
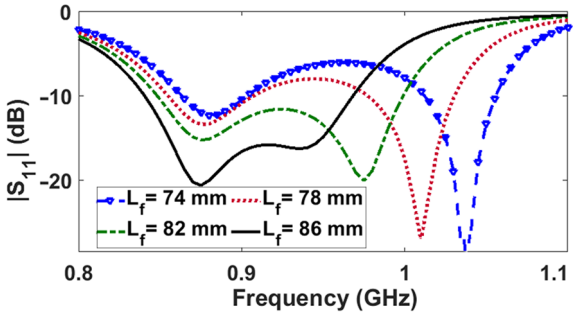
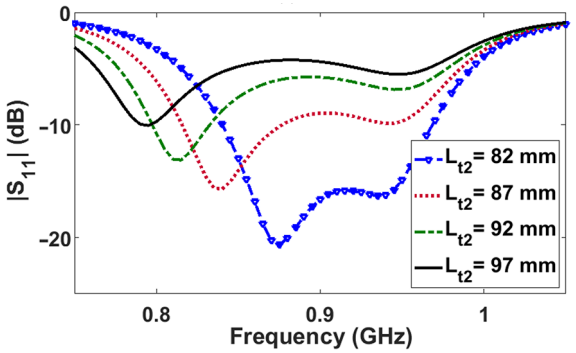


Figure 4. The Effect of length of ground plane on resonant frequency in designing narrow-band antenna, (**a**) different Ls while L = 100 mm, and (**b**) different L and Ls while L − Ls = 81.5 mm.

As demonstrated, the wide-band antenna has two resonant frequencies, and the parameters Lf and Lt2 adjust the second and first resonant frequencies, respectively. In fact, in Figure 5a, while Lt2 is constant, an increase in Lf, which is a part of the antenna trace shorted to the ground, shifts the second resonant frequency toward lower frequencies. On the other hand, the parameter Lt2, which is the open-ended part of the trace, can adjust the first resonant frequency. By adjusting these two parameters (i.e., Lf, and Lt2), the two resonant frequencies can be tailored close to each other to make the antenna wide-band. As shown in Figure 5b, for Lt2 = 82 mm, the two resonances are close enough to each other to create wide-band properties. To explain the wide-band mechanism of the proposed antenna for worldwide RFID applications, the surface currents are plotted at the first and second resonant frequencies in Figure 6. As shown, the lengths Lt2 and Lf create the first and second resonant frequencies, respectively, in agreement with Figure 5. As shown, in the first resonance frequency, the longer branch is radiating, which is obvious from its current density plot, and for the second resonance frequency, the shorter branch is radiating.



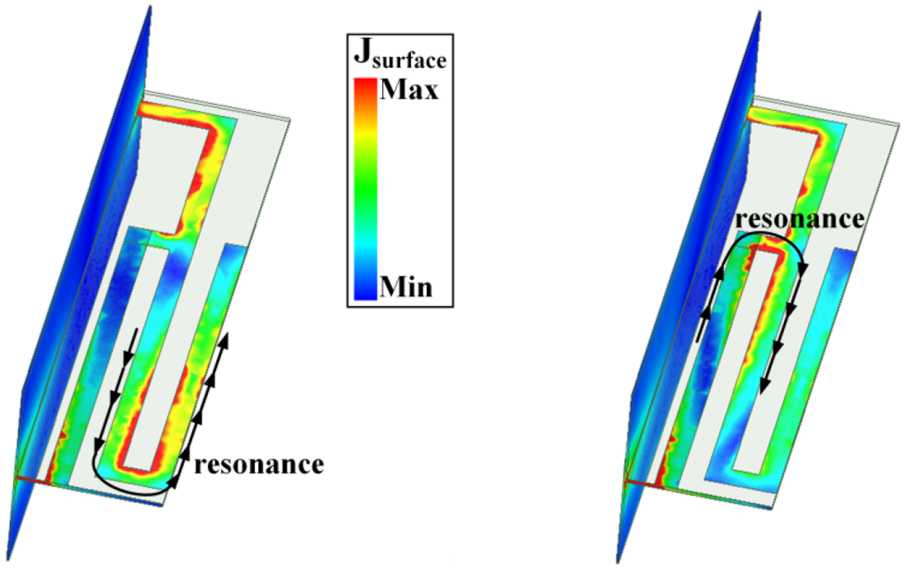
(**a**)



(**b**)

Figure 5. The effect of length of the antenna trace on resonant frequency in designing wideband antenna, (**a**) different Lf while L = 130 mm, Lt1 = 122 mm, and Lt2 = 82 mm, and (**b**) different Lt2 while L = 130 mm, Lt1 = 122 mm, and Lf = 86 mm.

Figure 7 illustrates the simulation-based plots of radiation efficiency vs. frequency of the both narrow-band and wide-band antennas. Both antennas represent an efficiency around 95% at the center frequency of 950 MHz. The product of radiation efficiency and gain of an antenna essentially gives its realized gain.



(**a**) (**b**)

Figure 6. Surface current of the wide-band monopole antenna at (**a**) first resonant frequency (873 MHz) and (**b**) second resonant frequency (938 MHz).

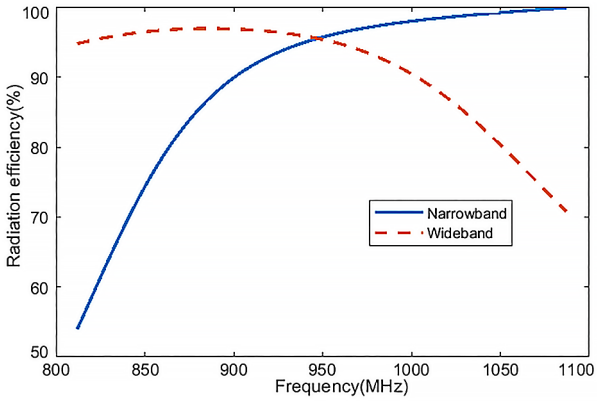
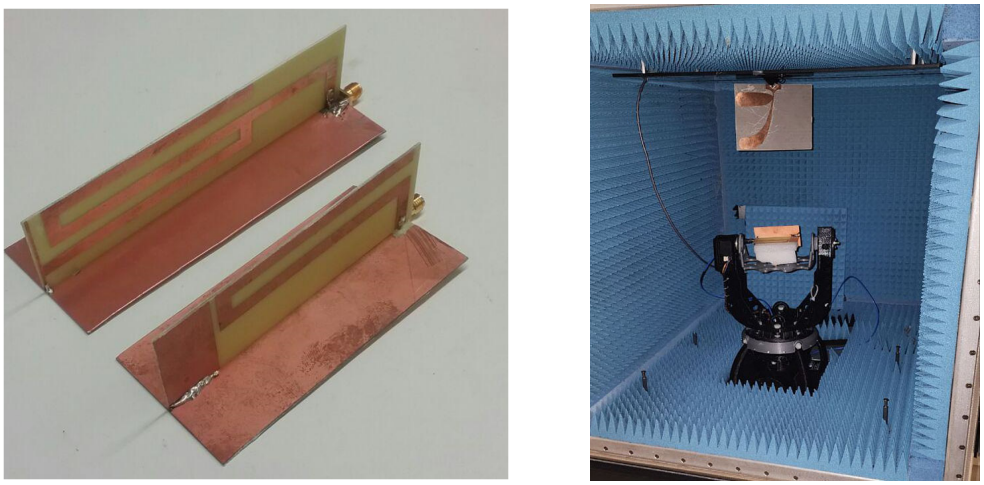


Figure 7. Radiation efficiency of both narrow-band and wide-band antennas.

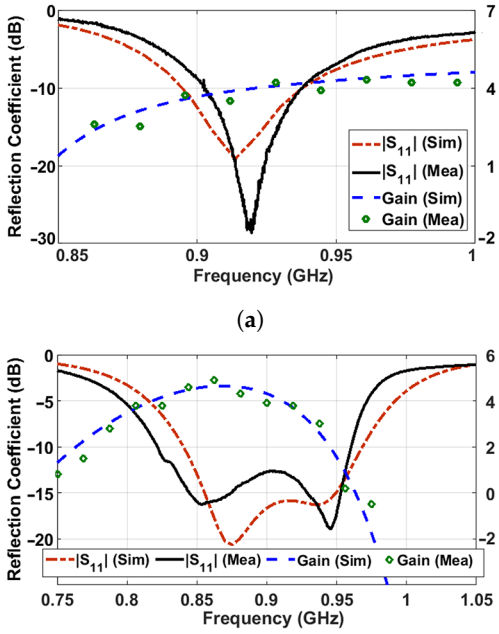
3. Experimental Results and Discussion

Figure 8a shows fabricated prototypes of the proposed narrow-band and wide-band monopole antennas for UHF RFID sensing applications. To examine the performance of the proposed antennas, the reflection coefficients of the fabricated antennas are first measured by a Vector Network Analyzer (VNA). As shown in Figure 9, the measured bandwidth of the proposed narrow-band antenna is from 902 MHz to 939 MHz (%4), which covers the desired RFID band of North America. The antenna pattern measurement tests were conducted in a near-field anechoic chamber, as shown in Figure 8b. The test setup included a precision scanning system and a vector network analyzer that collected the antenna's electromagnetic field in the near-field. The far-field radiation pattern of the antenna was calculated using the collected near-field data and a transformation algorithm. The gain plot shows that the gain at the center frequency is 4.2 dB for the narrow-band antenna and is 4.9 dB for the wide-band one. Thus, the realized gains could be easily calculated by multiplying the gain plots by the efficiency plots of Figure 7, giving 4.0 dB for the narrow-band and 4.6 dB for the wide-band.



(**a**) (**b**)

Figure 8. (**a**) Fabricated narrow-band and wide-band monopole antennas and (**b**) antenna pattern measurement setup.



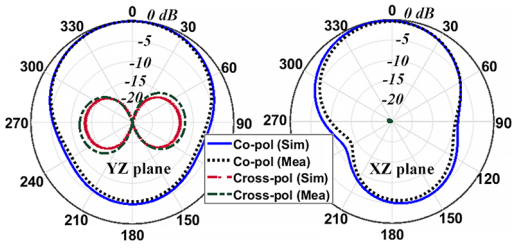
(**a**)

(**b**)

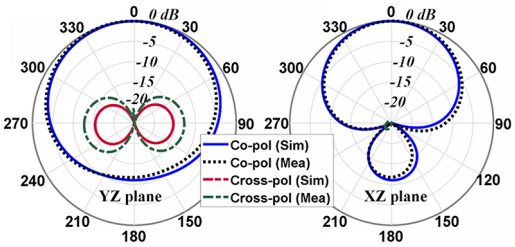
Figure 9. Reflection coefficient and antenna gain of the proposed antennas, (**a**) narrow-band monopole antenna, and (**b**) wide-band monopole antenna.

Similarly, as shown in Figure 9b, the measured bandwidth of the wideband antenna is over 822–961 MHz (%15.6), which covers the worldwide UHF RFID band. All simulation and measurement results are in good agreement. The slight difference between simulation and measurement results may be due to the fabrication tolerance. To investigate the radiation performance of the proposed antennas, the radiation patterns of the antennas are measured. The simulated and measured antenna gains for both antennas are plotted in Figure 10. It is evident that the antennas do not show significant backward radiation, caused by the presence of the ground plane. Figure 10 depicts the simulated and measured radiation patterns of both antennas in the YZ plane ($\phi = 90°$) and XZ plane ($\phi = 0°$) at 915 MHz. As seen, the half-power beam widths (HPBWs) of the YZ plane and XZ plane are 124° and 91° for the narrow-band antenna and 143° and 88° for the wide-band antenna, respectively. This shows the great coverage of the proposed antennas in the YZ plane, which is of great importance in RFID sensing applications, as discussed before. Also, for

the narrow-band antenna, the measured cross-polarization levels within the HPBWs of the YZ plane and XZ plane are at least 10 dB and 22 dB below the corresponding measured co-polarizations, respectively. For the wide-band antenna, in the YZ plane and XZ plane, the measured cross-polarizations within the HPBWs are nearly 9.5 dB and 22 dB under the corresponding measured co-polarization levels. These results show the linearity of the polarization of both proposed monopole antennas.



(**a**)



(**b**)

Figure 10. Radiation patterns of the proposed antennas at 915 MHz, (**a**) narrow-band monopole antenna, and (**b**) wide-band monopole antenna.

The proposed antennas can be integrated with the battery-less RFID flood sensor in [13] to be used in smart home applications. The integration with narrow-band antennas can be used in North America; however, the integration with the wide-band antenna is utilized worldwide. The configuration of the proposed antennas allows the integrated RFID sensors to be installed on dry walls or metallic cabinets.

In addition, our works are compared with some contemporary tag antennas for UHF bands in Table 1. It is evident that when compared with these recent UHF RFID antennas, our work can provide a promising directive gain. A careful examination of this table clarifies this fact that the antenna dimension is proportional to the efficacy of the antenna gain.

Table 1. Comparison between existing UHF naroowband tag antennas.

References	Antenna Type	Antenna Size mm^2	Radiation Pattern	Radiation Efficiency (%)	Realized Gain (dBi)
our work	Monopole	100 × 48	Directional	95	4
[27]	Monopole	83.625 × 83.625	Directional	76	2.7
[28]	Monopole	98.75 × 57	Omnidirectional	N/A	3.2
[29]	Dipole	101.2 × 10.5	Omnidirectional	N/A	3.14
[30]	Patch	50 × 50	Directional	N/A	−5.4

4. Conclusions

Two narrow-band and wide-band monopole antennas for the UHF band in North America and worldwide were proposed in this article. Both antennas were designed to be used for smart home wireless sensor nodes, as they have wide horizontal radiation patterns that provide broad reading coverage. As mentioned, the antennas have two ground planes, one in-plane and one vertical. The vertical ground helps for directive radiation, easy installation on walls, and protecting the RFID circuit against leakage from the antenna. The

experimental results, which were in good agreement with simulated ones, showed that the measured bandwidths of 4% (902–939 MHz) and 15.6% (822–961 MHz) were obtained for the proposed narrow-band and wide-band monopole antennas with the maximum measured gains of 4.2 dBi and 4.9 dBi, respectively.

Author Contributions: Conceptualization, M.M.H. and R.M.; methodology and design, M.M.H.; validation, M.M.H. and R.M.; formal analysis, M.M.H., S.P.J. and R.M.; writing—original draft preparation, M.M.H.; writing—review and editing, S.P.J. and R.M.; supervision, R.M.; project administration, R.M.; funding acquisition, R.M. All authors have read and agreed to the published version of the manuscript.

Funding: This research was funded by Alberta Innovates grant number RES0043828 and Natural Sciences and Engineering Research Council grant number RES0055189.

Data Availability Statement: The data that support the findings of this study are available from the corresponding author, R.M., upon request.

Conflicts of Interest: The authors declare no conflicts of interest.

References

1. Saghlatoon, H.; Mirzavand, R.; Honari, M.M.; Mousavi, P. Sensor Antenna Transmitter System for Material Detection in Wireless-Sensor-Node Applications. *IEEE Sens. J.* **2018**, *21*, 8812–8819. [CrossRef]
2. Liu, H.; Cheng, Y.; Yan, M. Electrically Small Loop Antenna Standing on Compact Ground in Wireless Sensor Package. *IEEE Antennas Wirel. Propag. Lett.* **2016**, *64*, 76–79. [CrossRef]
3. Varnoosfaderani, M.V.; Thiel, D.V.; Lu, J.W. A Wideband Slot Antenna in a Box for Wearable Sensor Nodes. *IEEE Antennas Wirel. Propag. Lett.* **2015**, *14*, 1494–1497. [CrossRef]
4. Wu, T.; Li, R.; Tentzeris, M.M. A Scalable Solar Antenna for Autonomous Integrated Wireless Sensor Nodes. *IEEE Antennas Wirel. Propag. Lett.* **2011**, *10*, 510–513. [CrossRef]
5. Khalid, N.; Iyer, A.K.; Mirzavand, R. A Batteryless Six-Port RFID-Based Wireless Sensor Architecture for IoT Applications. *IEEE Internet Things J.* **2022**, *9*, 18550–18558. [CrossRef]
6. Solar, H.; Beriain, A.; Rezola, A.; del Rio, D.; Berenguer, R. A 22-m Operation Range Semi-Passive UHF RFID Sensor Tag with Flexible Thermoelectric Energy Harvester. *IEEE Sens. J.* **2022**, *22*, 19797–19808. [CrossRef]
7. Sriram, V.P.; Raj, K.B.; Srinivas, K.; Pallathadka, H.; Sajja, G.S.; Gulati, K. An Extensive Systematic Review of RFID Technology Role in Supply Chain Management. In Proceedings of the International Conference on Signal Processing, Computing and Control (ISPCC), Solan, India, 7–9 October 2021; pp. 789–794.
8. Zhang, S.; Liu, X.; Liu, Y.; Ding, B.; Guo, S.; Wang, J. Accurate Respiration Monitoring for Mobile Users With Commercial RFID Devices. *IEEE J. Sel. Areas Commun.* **2021**, *39*, 513–525. [CrossRef]
9. Zhang, K.; Amineh, R.K.; Dong, Z.; Nadler, D. Microwave Sensing of Water Quality. *IEEE Access* **2019**, *7*, 69481–69493. [CrossRef]
10. Lehpamer, H. *RFID Design Principles*; Artech House: Norwood, MA, USA, 2007.
11. Saghlatoon, H.; Mirzavand, R.; Honari, M.M.; Mousavi, P. Investigation on Passive Booster for Improving Magnetic Coupling of Metal Mounted Proximity Range HF RFIDs. *IEEE Trans. Microw. Theory Tech.* **2017**, *65*, 3401–3408. [CrossRef]
12. Görtschacher, L.J.; Amtmann, F.; Muehlmann, U.; Merlin, E.; Priller, P.; Grosinger, J. Passive HF RFID Repeater for Communicating With Tags in Metal Housings. *IEEE Antennas Wirel. Propag. Lett.* **2020**, *19*, 1625–1629. [CrossRef]
13. Khalid, N.; Mirzavand, R.; Saghlatoon, H.; Honari, M.M.; Mousavi, P. A Three-Port Zero-Power RFID Sensor Architecture for IoT Applications. *IEEE Access* **2020**, *8*, 66888–66897. [CrossRef]
14. Alibakhshikenari, M.; Virdee, B.S.; Althuwayb, A.A.; Xu, K.D.; See, C.H.; Khan, S.; Park, I.; Falcone, F.; Limiti, E. Novel concentric hexagonal-shaped RFID tag antenna with T-shaped stub matching. *IEEE J. Radio Freq. Identif.* **2021**, *6*, 112–120. [CrossRef]
15. Basit, A.; Khattak, M.I.; Althuwayb, A.; Nebhen, J. Compact tri-band bandpass filter based on asymmetric step impedance resonators for WiMAX and RFID systems. *J. Electromagn. Eng. Sci.* **2021**, *21*, 316–321. [CrossRef]
16. Abdulhadi, A.E.; Abhari, R. Design and experimental evaluation of miniaturized monopole UHF RFID tag antennas. *IEEE Antennas Wirel. Propag. Lett.* **2012**, *13*, 248–251. [CrossRef]
17. Tan, J.I.; Lee, Y.H.; Lim, E.H.; Bong, F.L.; Chung, B.K. A Low-Profile Top-Loaded Monopole Antenna for On-Metal RFID Tag Design. *IEEE J. Radio Freq. Identif.* **2024**, *8*, 448–457. [CrossRef]
18. Aggarwal, I.; Tripathy, M.R.; Pandey, S.; Mittal, A. A Dual band Monopole Antenna For RFID Applications. In Proceedings of the 2021 IEEE International Conference on RFID Technology and Applications (RFID-TA), Delhi, India, 6–8 October 2021; pp. 67–70.
19. Asci, C.; Wang, W.; Sonkusale, S. *Security Monitoring System Using Magnetically-Activated RFID Tags*; IEEE: Rotterdam, The Netherlands, 2020; pp. 1–4.
20. Wang, Y.; Yan, S. A Compact In-Band Full Duplexing Antenna With Quasi-Isotropic Radiation Pattern for IoT-Based Smart Home and Intravehicle Wireless Communication Applications. *IEEE Internet Things J.* **2022**, *9*, 16689–16700. [CrossRef]

21. Khalili, H.F.; Lemey, S.; Caytan, O.; Deckmyn, T.; Agneessens, S.; Ginste, D.V.; Rogier, H. Biodegradable Dual Semicircular Patch Antenna Tile for Smart Floors. *IEEE Antennas Wirel. Propag. Lett.* **2019**, *18*, 368–372. [CrossRef]
22. Hu, Z.; Shen, Z.; Wu, W.; Lu, J. Low-Profile Top-Hat Monopole Yagi Antenna for End-Fire Radiation. *IEEE Trans. Antennas Propag.* **2015**, *63*, 2851–2857. [CrossRef]
23. Zhang, X.; Sun, F.; Zhang, G.; Hou, L. Compact UHF/VHF Monopole Antennas for CubeSats Applications. *IEEE Access* **2020**, *8*, 133360–133366. [CrossRef]
24. Zheng, M.; Wang, H.; Hao, Y. Internal Hexa-Band Folded Monopole/Dipole/Loop Antenna with Four Resonances for Mobile Device. *IEEE Trans. Antennas Propag.* **2012**, *60*, 2880–2885. [CrossRef]
25. Li, Y.; Podilchak, S.K.; Anagnostou, D.E.; Constantinides, C.; Walkinshaw, T. Compact Antenna for Picosatellites Using a Meandered Folded-Shorted Patch Array. *IEEE Antennas Wirel. Propag. Lett.* **2020**, *19*, 477–481. [CrossRef]
26. Zhang, H.; Li, M.; Yang, F.; Xu, S.; Zhou, H.; Yang, Y.; Chen, L. A Low-Profile Compact Dual-Band L-Shape Monopole Antenna for Microwave Thorax Monitoring. *IEEE Antennas Wirel. Propag. Lett.* **2020**, *19*, 448–452. [CrossRef]
27. Abdulhadi, A.E.; Abhari, R. Passive UHF RFID printed monopole tag antenna for identification of metallic objects. In Proceedings of the 2012 IEEE International Symposium on Antennas and Propagation, Chicago, IL, USA, 8–14 July 2012; pp. 1–2.
28. Ramirez, R.A.; Rojas-Nastrucci, E.A.; Weller, T.M. UHF RFID tags for on-/off-metal applications fabricated using additive manufacturing. *IEEE Antennas Wirel. Propag. Lett.* **2017**, *16*, 1635–1638. [CrossRef]
29. Hussain, M.; Amin, Y.; Lee, K.G. A compact and flexible UHF RFID tag antenna for massive IoT devices in 5G system. *Sensors* **2020**, *20*, 5713. [CrossRef]
30. Zhao, L.; Ma, Y.; Meng, W.; Peng, K.; Liu, K. Bendable folded-patch antenna with resonant ring manufactured based on foam support and PET substrate for on-metal UHF RFID. *IEEE J. Radio Freq. Identif.* **2023**, *7*, 591–600. [CrossRef]

Disclaimer/Publisher's Note: The statements, opinions and data contained in all publications are solely those of the individual author(s) and contributor(s) and not of MDPI and/or the editor(s). MDPI and/or the editor(s) disclaim responsibility for any injury to people or property resulting from any ideas, methods, instructions or products referred to in the content.